World Academy of Science, Engineering and Technology
International Journal of Mechanical and Mechatronics Engineering
Vol:5, No:10, 2011

Analysis of Residual Strain and Stress Distributions in High Speed Milled Specimens using an Indentation Method

Felipe V. Díaz, Claudio A. Mammana, Armando P. M. Guidobono and Raúl E. Bolmaro

***Abstract*—**Through a proper analysis of residual strain and stress distributions obtained at the surface of high speed milled specimens of AA 6082–T6 aluminium alloy, the performance of an improved indentation method is evaluated. This method integrates a special device of indentation to a universal measuring machine. The mentioned device allows introducing elongated indents allowing to diminish the absolute error of measurement. It must be noted that the present method offers the great advantage of avoiding both the specific equipment and highly qualified personnel, and their inherent high costs. In this work, the cutting tool geometry and high speed parameters are selected to introduce reduced plastic damage. Through the variation of the depth of cut, the stability of the shapes adopted by the residual strain and stress distributions is evaluated. The results show that the strain and stress distributions remain unchanged, compressive and small. Moreover, these distributions reveal a similar asymmetry when the gradients corresponding to conventional and climb cutting zones are compared.

***Keywords*—**Residual strain, residual stress, high speed milling, indentation methods, aluminium alloys.

NOMENCLATURE

A	elongation (%)
d	depth of cut (mm)
E	longitudinal elastic modulus (GPa)
f	feed rate (mm/rev)
F_{tx}	tangential force component at the x direction (N)
F_{ty}	tangential force component at the y direction (N)
HV0.5	Vickers micro-hardness (test load: 500 gf)
k_1, k_2	elastic constants
$m_{\varepsilon x}$	gradient of the ε_x component along the axis $x = 0$ (1/mm)
$m_{\varepsilon y}$	gradient of the ε_y component along the axis $y = 0$ (1/mm)
$m_{\sigma x}$	gradient of the σ_x component along the axis $x = 0$ (MPa/mm)
$m_{\sigma y}$	gradient of the σ_y component along the axis $y = 0$ (MPa/mm)
N	number of measurements
Sx	standard deviation (μm)
V	cutting speed (m/min)
V_x	cutting speed component at the x direction (m/min)
V_y	cutting speed component at the y direction (m/min)
X_b, X_a	distances between indents located at the x direction, before and after the distension (mm)
Y_b, Y_a	distances between indents located at the y direction, before and after the distension (mm)
α	clearance angle (deg)
γ	rake angle (deg)
ε_x	residual strain component at the x direction
ε_y	residual strain component at the y direction
υ	Poisson's ratio
σ_x	residual stress component at the x direction (MPa)
σ_y	residual stress component at the y direction (MPa)
σ_u	ultimate tensile strength (UTS) (MPa)
$\sigma_{y\,0.2}$	yield strength (MPa)
χ	entrance angle (deg)
Δdn_b, Δdn_a	nominal errors, before and after the distension, respectively (μm)
Δds_b, Δds_a	statistical errors, before and after the distension, respectively (μm)
ΔX_b, ΔX_a	absolute errors inherent to the distances X_b and X_a, respectively (μm)
ΔY_b, ΔY_a	absolute errors inherent to the distances Y_b and Y_a, respectively (μm)
$\Delta\varepsilon x$	absolute error of the ε_x component
$\Delta\varepsilon y$	absolute error of the ε_y component
$\Delta\sigma x$	absolute error of the σ_x component (MPa)
$\Delta\sigma y$	absolute error of the σ_y component (MPa)

F. V. Díaz (corresponding author) and C. A. Mammana are with the Departamento de Iingeniería Electromecánica and the Departamento de Ingeniería Industrial, Facultad Regional Rafaela, Universidad Tecnológica Nacional, Bvd Roca 989, 2300 Rafaela, Argentina (phone: + 54 3492 422880; fax: + 54 3492 432710; e-mail: felipe.diaz@frra.utn.edu.ar, claudio.mammana@frra.utn.edu.ar).

A. P. M. Guidobono is with the División Metrología Dimensional, Centro Regional Rosario (INTI) Ocampo y Esmeralda, 2000 Rosario, Argentina (e-mail: armandog@inti.gob.ar).

R. E. Bolmaro is with the Instituto de Física Rosario (CONICET – UNR) Bvd 27 de Febrero 210 bis, 2000 Rosario, Argentina (e-mail: bolmaro@ifir-conicet.gov.ar).

I. INTRODUCTION

THE universal measuring machines (UMMs) are used in industry for performing high precision dimensional measurements in different types of machine and structure components [1,2]. Some years ago, these machines started to be considered an important part of industrial quality systems, resulting in lower inspection costs and higher productivity. These types of machines are employed due to their speed, accuracy and flexibility, fulfilling both the traditional function of rejecting out-of-specification components, as well as the

one of supplying product geometry information that can be used to improve the manufacturing process [3].

Clearly, these machines were not designed for residual stress measurements [4-6]. However, a method based on the modification of the distance between indent pairs was recently developed to determine residual stresses using a UMM [7]. The distance change occurs when the component is subjected to a distension procedure to relieve the residual stresses. It must be noted that this method has the great advantage of being simple and inexpensive because it does not require specific personnel and equipment.

High-speed machining (HSM) [8] uses a technology that enables decreasing production costs by increasing the values of processing parameters, such as feed rate and cutting speed. HSM offers many benefits compared to conventional machining [9] such as reduced number of technological operations, decreased production flow time and longer service time of tools [10]. In addition, HSM generates an equivalent - or better- surface finish, form, and size accuracy. However, high-speed machined parts can fail prematurely due to the development of residual stresses [11,12].

The purpose of this paper is to evaluate the performance of an improved indentation method through the analysis of residual strain and stress distributions, which are obtained from the evaluation of high speed milled specimens of AA 6082-T6 aluminium alloy. This method includes an indentation device, which is specially incorporated to a UMM. From the integration of this device to the measuring machine, the absolute error of measurement can be highly reduced. The specimens were subjected to face milling operations, which were carried out in a vertical CNC milling machine. Regarding the process parameters, both the feed rate and cutting velocity were fixed, and the depth of cut was varied to evaluate the stability of the residual strain and stress distributions. It is important to note that high speed milling operations pose a series of technological challenges that are not always solved in a right way. Moreover, there is little literature on residual strain and stress distributions introduced at the surface of AA 6082-T6 aluminium alloy. This paper also includes a meticulous analysis of the propagation of errors inherent in measurements of indent coordinates. This analysis allowed corroborating that residual strains and stresses were obtained from much reduced errors. The residual stresses were calculated through the mentioned measurements of coordinates, using a model for plane stress state [13]. Finally, from strain and stress gradients it was possible to analyze the machined zones corresponding to both conventional and climb cutting.

II. Experimental Procedure

The above-mentioned method of indent pairs is presented in Ref. 7. In the first place, an indent distribution is introduced at the specimen surface using a micro-hardness tester. Secondly, the distances between indent pairs are measured before and after a stress-relieving treatment using a UMM. In this work, the measurement procedure does not require a micro-hardness tester. The indent distribution is introduced using an indentation device, which is integrated to the UMM. Figure 1 shows the indentator of the device making contact with the milled surface of the specimen. It should be noted that the body of the device is made up of a system of thin elastic strips that enables to regulate the indentation load. In addition, an electronic sensor allows calibrating the depth of the indent with high accuracy. Through the use of the mentioned device it is possible to increase the accuracy of both introduction and optical localization of the indent distribution. Besides, this device allows generating elongated indents, which help to reduce the uncertainty of specimen repositioning after the distension procedure. Figure 2 shows an isometric drawing and a cross-section view of an elongated indent. It is important to mention that in a previous study [14] the maximum absolute errors corresponding to pyramidal and elongated indent distances were compared; for a nominal distance of 28 mm, the obtained values were ± 1.51 μm and ± 0.26 μm, respectively. The reduction of the distance measurement error allowed a substantial decrement of the absolute error of the stress components, which enabled to extend the sensitivity of the method below 6% of the yield stress.

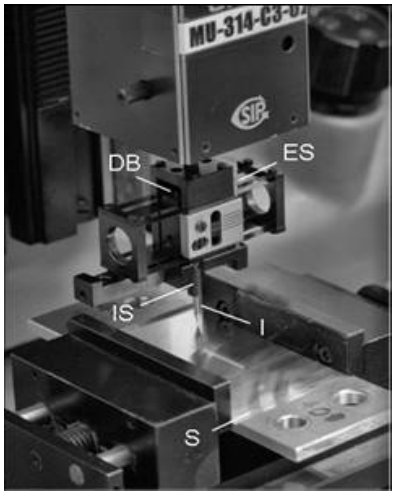

Fig. 1 Picture of indentator-specimen interaction: (DB) device body, (ES) elastic strips, (I) indentator, (IS) indentator support, (S) specimen

The dimensions of high speed machined specimens were 110 x 40 x 4 mm³. The evaluated material in this work corresponds to a rolled aluminium alloy AA 6082-T6. It must be noted that this material is used for structural applications in the marine and transportation industries, as well as for machined precision components in the automotive industry. The values corresponding to its chemical composition and mechanical properties are detailed in Tables I and II, respectively. It is important to note that before milling tests, each specimen was subject to a simple stress-relieving treatment using an annealing temperature of 573 K for a

period of 80 minutes. High speed milling tests were carried out using a face mill of 63 mm in diameter. Five tungsten carbide inserts (Palbit SEHT 1204 AFFN-AL SM10) were incorporated to the mentioned face mill. In Table III, both the insert geometry and high speed parameters are reported. The face mill was attached to the spindle of a Clever CMM-100 vertical CNC milling machine. It is worth noting that this is a very rigid machine tool that includes powerful axis drives and large precision ball screws. Figure 3(a) shows a superior view of the high-speed milling operation. In addition, Fig. 3(b) shows a schematic diagram of the milled surface, where two zones -conventional and climb cutting- can be differentiated.

TABLE I
CHEMICAL COMPOSITION OF THE INVESTIGATED ALUMINIUM ALLOY

Chemical composition (wt %)							
Mg	Si	Mn	Fe	Zn	Cr	Cu	Al
0.9	0.9	0.6	0.5	0.2	0.22	0.15	balance

TABLE II
ELASTIC AND MECHANICAL PROPERTIES OF THE INVESTIGATED ALLOY

Properties					
σ_u (MPa)	$\sigma_{y_{0.2}}$ (MPa)	A (%)	HV0.5	E (GPa)	ν
341	314	11	108	70	0.33

TABLE III
INSERT GEOMETRY AND CUTTING PARAMETERS

Rake angle	Clearance angle	Entrance angle	Cutting speed	Feed rate	Depth of cut
γ (°)	α (°)	χ (°)	V (m/min)	f (mm/rev)	d (mm)
45	7	45	1000	0.2	1.00 – 1.25

On each machined surface, an indent distribution was introduced. Each indent distribution allowed to determine the residual strain and stress components in several points corresponding to both symmetry axes ($x = 0$ and $y = 0$ in Fig. 3(b)). The coordinates of indents were measured, before and after the distension treatment, using a measuring machine GSIP MU-314. The measurements were carried out within a temperature range of 20 ± 0.2 °C. Finally, the above-mentioned distension treatment was also performed for a period of 80 minutes at a temperature of 573 K.

It should be noted that if the distension treatment is performed below the recrystallization temperature [15], the dimensional changes at the specimen will be governed only by the elastic relaxation of the lattice (the plastic flow activated by temperature is highly localized and it can be reduced to the annihilation of vacancies and dislocations of opposite sign and to rearrangement of dislocations into lower-energy configurations). In addition, if the specimen geometry is simple, the thickness is small, and the cooling rate is slow, it is possible to avoid the development of thermal residual stresses.

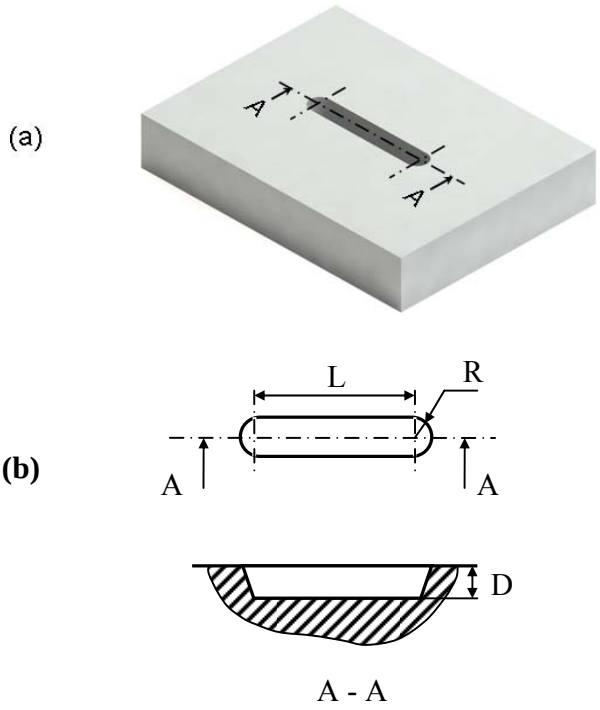

Fig. 2 (a) Isometric drawing and (b) cross-section view of an elongated indent: (L) indent length, (R) end radius, (D) indent depth

III. ERROR EVALUATION AND PROPAGATION

Through an adequate distribution of four elongated indents, it is possible to obtain the orthogonal components of the residual strain

$$\varepsilon_x = \frac{X_b}{X_a} - 1$$

$$\varepsilon_y = \frac{Y_b}{Y_a} - 1 \quad (1)$$

where X_b and X_a are the distances between indents whose longitudinal axes are parallel to the feed direction, before and after the distension procedure, respectively. In addition, Y_b and Y_a correspond to the distances between indents whose longitudinal axes are normal to the feed direction, before and after the same distension procedure, respectively.

The absolute error of these distances, before and after the mentioned distension procedure, can be expressed from nominal and statistical errors as [16]

$$\Delta X_b \approx \Delta Y_b = \sqrt{\Delta d_{n_b}^2 + \Delta d_{s_b}^2}$$

$$\Delta X_a \approx \Delta Y_a = \sqrt{\Delta d_{n_a}^2 + \Delta d_{s_a}^2} \quad (2)$$

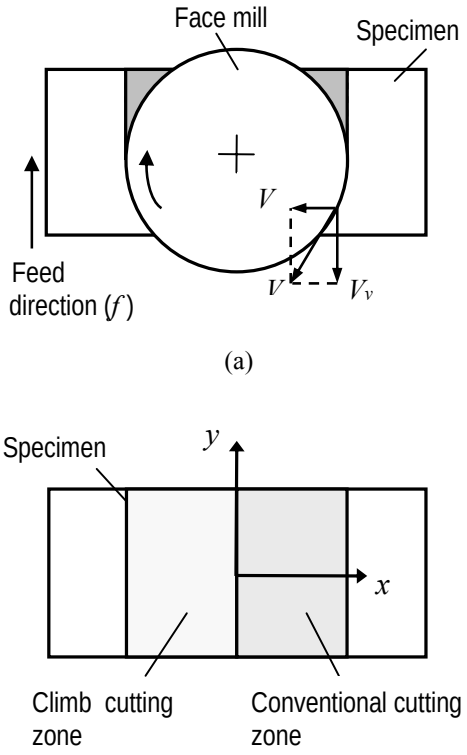

Fig. 3 (a) Diagram of the high-speed milling operation. (b) Milled surface

where

$$\Delta d_{n_b} = \sqrt{\Delta d_{ile}^2 + \Delta d_{ca}^2}$$

$$\Delta d_{n_a} = \sqrt{\Delta d_{ile}^2 + \Delta d_{ca}^2 + \Delta d_{in}^2}$$

$$\Delta d_{s_b} \approx \Delta d_{s_a} = S_x / \sqrt{N} \tag{3}$$

and where Δd_{ile} is the instrument limit of error (ILE), Δd_{ca} is the calibration error, Δd_{in} is the interaction error S_x is the standard deviation or mean square error and N is the number of measurements. It must be noted that Δd_{ile} corresponds to the smallest reading that the operator can make with the measurement machine and Δd_{ca} represents the machine calibration uncertainty. In our case, the latter is very small, and besides, it can be considered as negligible because the distance between indents is obtained from the subtraction of two near coordinates. On the other hand, Δd_{in} is the error corresponding to the interaction between the measurement procedure and the measured object. In our case, this corresponds to the uncertainty of specimen repositioning after the stress-relieving treatment. Table IV shows the errors corresponding to the performed measurements. It should be noted that six measurements of each indent coordinate were carried out to obtain the statistical errors.

Then, the absolute errors of the orthogonal components of the residual strain can be obtained from the errors corresponding to the indent distances through [16]

$$\Delta\varepsilon_x = \sqrt{\left(\frac{d\varepsilon_x}{dX_b}\right)^2 \cdot \Delta X_b^2 + \left(\frac{d\varepsilon_x}{dX_a}\right)^2 \cdot \Delta X_a^2} = \sqrt{\left(\frac{\Delta X_b}{X_a}\right)^2 + \left(\frac{\Delta X_a}{X_a^2}\right)^2 \cdot X_b^2}$$

$$\Delta\varepsilon_y = \sqrt{\left(\frac{d\varepsilon_y}{dY_b}\right)^2 \cdot \Delta Y_b^2 + \left(\frac{d\varepsilon_y}{dY_d}\right)^2 \cdot \Delta Y_a^2} = \sqrt{\left(\frac{\Delta Y_b}{Y_a}\right)^2 + \left(\frac{\Delta Y_a}{Y_a^2}\right)^2 \cdot Y_b^2} \tag{4}$$

As mentioned above, if the distension procedure is performed below the recrystallization temperature, the dimensional change of the evaluated surface will be caused by the elastic relaxation of the lattice. Therefore, if the evaluated surface is considered to be under plane-stress conditions [13], the orthogonal components of the residual stress can be expressed for isotropic, linear elastic materials as

$$\sigma_x = k_1 \cdot \varepsilon_x + k_2 \cdot \varepsilon_y$$

$$\sigma_y = k_1 \cdot \varepsilon_y + k_2 \cdot \varepsilon_x \tag{5}$$

where $k_1 = E / (1 - \upsilon^2)$, $k_2 = \upsilon \cdot k_1$, E is the longitudinal elastic modulus and υ is the Poisson's ratio. Then, the absolute errors of these components can be obtained from the errors corresponding to the orthogonal components of the residual strain [16]

$$\Delta\sigma_x = \sqrt{\left(\frac{d\sigma_x}{d\varepsilon_x}\right)^2 \cdot \Delta\varepsilon_x^2 + \left(\frac{d\sigma_x}{d\varepsilon_y}\right)^2 \cdot \Delta\varepsilon_y^2} = \sqrt{k_1^2 \cdot \Delta\varepsilon_x^2 + k_2^2 \cdot \Delta\varepsilon_y^2}$$

$$\Delta\sigma_y = \sqrt{\left(\frac{d\sigma_y}{d\varepsilon_x}\right)^2 \cdot \Delta\varepsilon_x^2 + \left(\frac{d\sigma_y}{d\varepsilon_y}\right)^2 \cdot \Delta\varepsilon_y^2} = \sqrt{k_2^2 \cdot \Delta\varepsilon_x^2 + k_1^2 \cdot \Delta\varepsilon_y^2} \tag{6}$$

Finally, from (4) and (6), the absolute errors of the residual strain and stress components were ± 0.001% and ± 0.9 MPa, respectively. It is important to observe that typical errors from X-ray diffraction technique and hole-drilling method are ± 20 MPa and ± 50 MPa, respectively [6].

TABLE IV
MEASUREMENT ERRORS

ILE (μm)	Interaction error (μm)	Nominal errors (μm)		Statistical errors (μm)	
Δd_{ile}	Δd_{in}	Δd_{n_b}	Δd_{n_a}	Δd_{s_b}	Δd_{s_a}
0.10	0.19	0.10	0.22	0.13	0.13

IV. Results and Discussion

The component of the residual strain ε_x was evaluated in several points of the symmetry axis $x = 0$. It is worth noting that this component is normal to the feed direction. Figure 4(a) shows the distributions of this component for different depths of cut. As it can be seen, the variation in the depth of cut does not introduce changes in the shape of the distribution. Moreover, a decrease in the distribution level is produced when the depth of cut increases. Figure 4(b) shows the component of the residual stress σ_x, which was evaluated along the same symmetry axes $x = 0$. The distributions are very much alike those shown in Fig. 4(a) (the shape is the same and the level decreases with the augmentation of the depth of cut).

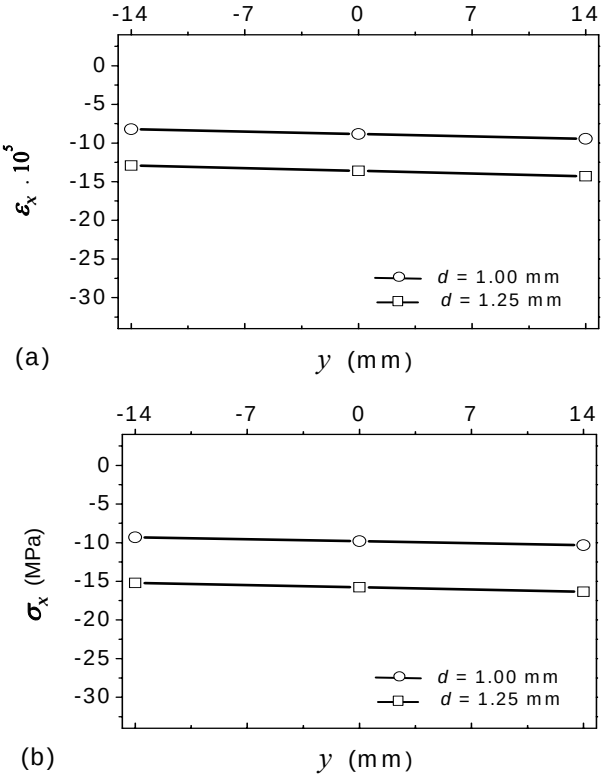

Fig. 4 Distributions of the components (a) ε_x and (b) σ_x along the axis $x = 0$ (cutting speed: $V = 1000$ m/min, feed rate: $f = 0.2$ mm/rev)

The other component of the residual strain ε_y, which is parallel to the feed direction, was evaluated along the symmetry axis $y = 0$. Figure 5(a) shows the distributions corresponding to this component. These distributions show a V-shaped profile, with the minimum value situated at the axis centre. As expected, the increase in the depth of cut generated more compressive strains. In addition, Fig. 5(b) shows the component of the residual stress σ_y along the same axis. Both distributions have the same shape, and besides, they show a great similarity with those corresponding to the component ε_y.

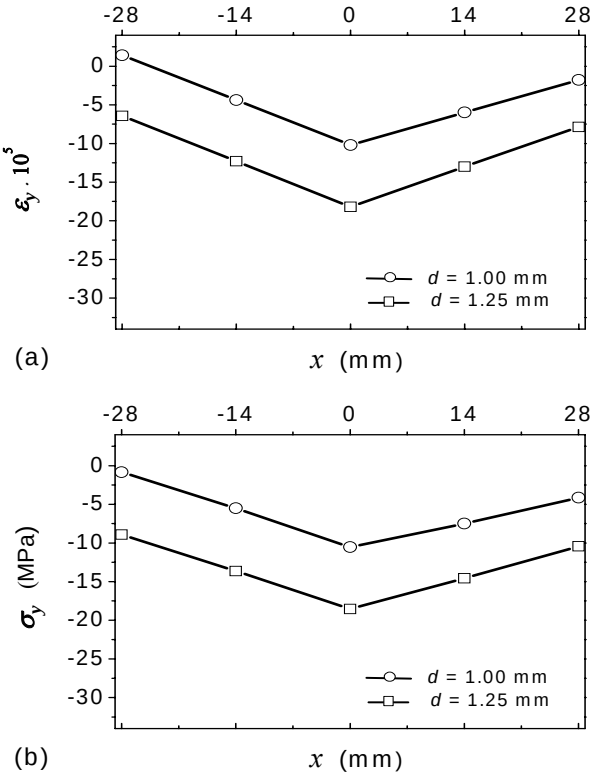

Fig. 5 Distributions of the components (a) ε_y and (b) σ_y along the axis $y = 0$ (cutting speed: $V = 1000$ m/min, feed rate: $f = 0.2$ mm/rev)

It can be observed that, for the selected process parameters, the obtained residual strains and stresses show very low values, which help to evaluate the proposed measurement procedure. Moreover, these strains and stresses are compressive, which is appropriate for the case of having to withstand fatigue load cycles [17,18]. The shape of the strain and stress distributions, which is linear (very low gradient) along the axis $x = 0$ (Fig. 4), could respond to the strong influence of the component of the cutting tangential force F_{tx} in the process of local plastic deformation [14]. It is important to note that this component is constant along the symmetry axis $x = 0$, and besides, the other component F_{ty} is zero along the same axis. Table V shows the values corresponding to the strain and stress gradients along the axis $x = 0$. For both variables, the differences between gradients resulted to be similar, and lower than 11%. These small differences help to corroborate the good performance of the present method.

TABLE IV
Strain and Stress Gradients

Depth of cut (mm)	Gradients	
	$m_{\varepsilon x} \cdot 10^5$ (1/mm)	$m_{\sigma x}$ (MPa/mm)
1.00	-0.0446	-0.0361
1.25	-0.0500	-0.0404

On the other hand, the components shown along the axis y

= 0 (Fig. 5) have a V-shaped profile. This type of profile could also be induced by the component F_{tx}, which shows a symmetrical distribution with the minimum value at the axis centre and the maximum values at the axis ends [14]. However, it can be observed that this V-shaped profile is somewhat asymmetrical: the gradients corresponding to $x < 0$ are slightly higher than those corresponding to $x > 0$. This asymmetry can be explained as follows. For $x > 0$, the feed rate f and the component of cutting speed V_y have opposite directions (conventional cutting), and for $x < 0$, both f and V_y have the same direction (climb cutting). The gradients corresponding to $x > 0$ are slightly lower because conventional cutting generates slightly more compressive strains and stresses than climb cutting. It occurs that conventional cutting is so light at the beginning of the cutting action that the inserts slide on the specimen surface until sufficient pressure build up and they begin to cut. This introduces a small additional increase of local plastic deformation at the milled surface, which does not occur in the case of climb cutting [14]. Figure 6 shows the values of the gradients in both machined zones. As expected, the values corresponding to the conventional cutting zone ($x > 0$) show bigger differences than those corresponding to the climb cutting zone ($x < 0$). In addition, the differences between the absolute values corresponding to both zones decrease with the augmentation of the depth of cut. For instance, the differences between the absolute values of the stress gradients corresponding to climb and conventional cutting were 0.118 MPa/mm and 0.054 MPa/mm, for depths of cut d = 1.00 mm and d = 1.25 mm, respectively. It is worth mentioning that although these differences resulted to be very small, the proposed method is capable of detecting them, differentiating between gradients of climb and conventional cutting.

V. Conclusion

The method of elongated indents used in this work allowed determining residual strains and stresses with errors of ± 0.001% and ± 0.9 MPa, respectively. Different strain and stress distributions were evaluated along the specimen symmetry axes, which are parallel and normal to the feed direction. The distributions resulted to be compressive and very low. In all cases, the variation in the depth of cut did not produce modifications in the shape of the distributions. In addition, this variation also generated a small decrease in the level of each distribution. Particularly, the distributions revealed a similar asymmetry degree when the zones of conventional and climb cutting were compared. The patterns showed by all distributions may respond to mechanical effects generated by the component of the cutting tangential force that is normal to the feed direction. Finally, the meticulous analysis and evaluation of the strain and stress gradients performed in this work allowed the corroboration of the good performance of the presented indentation method.

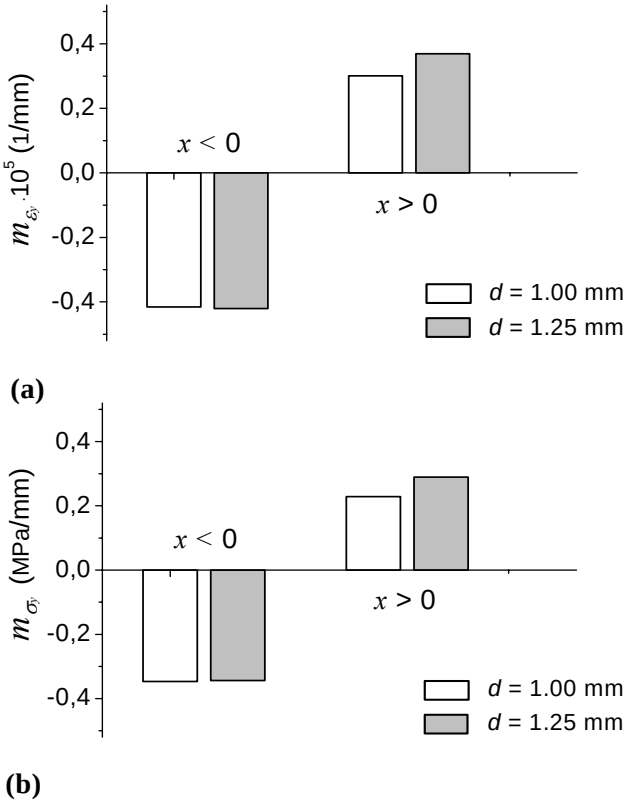

Fig. 6 Strain and stress gradients along the axis $y = 0$

Acknowledgment

The authors wish to express their sincere thanks to Eduardo Cravero and Silvio Acosta for their assistance during HSM test phase. This work was supported by the Departamento de Ingeniería Electromecánica and the Departamento de Ingeniería Industrial, Facultad Regional Rafaela, Universidad Tecnológica Nacional.

References

[1] C. L. Dotson, R. Harlow, and R. L. Thompson, Fundamentals of Dimensional Metrology. New York: Thompson Delmar Learning, 2003.
[2] M. A. Curtis, and F. T. Farago, Handbook of Dimensional Measurement. New York: Industrial Press Inc., 2007.
[3] J. A. Bosch (Ed.), Coordinate Measuring Machines and Systems. New York: Marcel Deckker, Inc., 1995.
[4] J. Lu (Ed.), Handbook of Measurement of Residual Stresses. Lilburn, Georgia: Fairmont Press Inc., 1996.
[5] R. E. Rowlands, "Residual stresses," in Handbook on Experimental Mechanics, A. S. Kobayashi, Ed. New Jersey: Prentice-Hall, 1987, pp. 768-813.
[6] P.J. Withers, and H. K. Bhadeshia, "Residual stress" Part 1 – Measurement techniques, Mater. Sci. Technol., vol. 17, pp. 355-365, 2001.
[7] J.E. Wyatt, and J.T. Berry, "A new technique for the determination of superficial residual stresses associated with machining and other manufacturing processes," J. Mater. Proc. Tech., vol. 171, pp. 132-140, 2006.
[8] H. Schulz, High Speed Machining. Munich: Carl Hanser, 1996.
[9] E. M. Trent, Metal Cutting. London: Butterworth/Heinemann, 1991.
[10] R. L. King (Ed.), Handbook of High Speed Machining Technology. New York: Chapman and Hall, 1985.

[11] A. L. Mantle, D. K. Aspinwall, "Surface integrity of a high speed milled gamma titanium aluminide," J. Mater. Proc. Tech., vol. 118, pp. 143-150, 2001.
[12] P. J. Withers, "Residual stress and its role in failure," Rep. Prog. Phys., vol. 70, pp. 2211-2264, 2007.
[13] S. P. Timoshenko, and J. N. Goodier, Theory of Elasticity, 3rd edn, New York: McGraw-Hill, 1970.
[14] F. V. Díaz, R. E. Bolmaro, A. P. M. Guidobono, and E. F. Girini, "Determination of residual stresses in high speed milled aluminium alloys using a method of indent pairs," Exp. Mech., vol. 50, pp. 205-215, 2010.
[15] W. Mao, "Recrystallization and grain growth," in Handbook of Aluminum, vol. 1, Physical Metallurgy and Processes, G. E. Totten, and D. S. MacKenzie, Ed. New York: Marcel Dekker Inc., 2003, pp. 211-258.
[16] P. R. Bevington, and D. K. Robinson, Data reduction and error analysis for the physical sciences, New York: McGraw-Hill, 2002.
[17] A. M. Korsunsky, G. M. Regino, D. P. Latham, H. Y. Li, and M. J. Walsh, "Residual stresses in rolled and machined nickel alloy plates: synchrotron X-ray diffraction measurement and three-dimensional eigenstrain analysis," J. strain analysis, vol. 42, pp. 1-12, 2007.
[18] D. W. Schwach, and Y. B. Guo, "A fundamental study on the impact of surface integrity by hard turning on rolling contact fatigue," Int. J. Fatigue, vol. 28, pp. 1838-1844, 2006.